Noncollinear magnetic order induced by Dzyaloshinskii–Moriya interaction in oxygen-assisted Pt nanojunctions

2016 Nanotechnology 27 475202

(http://iopscience.iop.org/0957-4484/27/47/475202)

IOP Publishing Nanotechnology
Nanotechnology 27 (2016) 475202 (7pp) doi:10.1088/0957-4484/27/47/475202

Noncollinear magnetic order induced by Dzyaloshinskii–Moriya interaction in oxygen-assisted Pt nanojunctions

J R Yuan[1], X H Yan[1,2,3], Y Xiao[1], Y D Guo[2,3] and C J Dai[1]

[1] College of Science, Nanjing University of Aeronautics and Astronautics, Nanjing 210016, People's Republic of China
[2] College of Electronic Science and Engineering, Nanjing University of Posts and Telecommunications, Nanjing 210023, People's Republic of China
[3] Key Laboratory of Radio Frequency and Micro-Nano Electronics of Jiangsu Province, Nanjing 210023, People's Republic of China

E-mail: yanxh@njupt.edu.cn and fryxiao@nuaa.edu.cn

Received 23 May 2016, revised 16 September 2016
Accepted for publication 30 September 2016
Published 24 October 2016

Abstract

Motivated by recent measurement of the magnetism and conductance of the oxygen-assisted Pt nanojunctions, we performed first principle calculations of the magnetic order and electronic transport by explicitly including fully relativistic effects. Our results show that the spin alignment is a cycloidal spiral feature attributed to the Dzyaloshinskii–Moriya interaction, which indicates that the observed magnetism in experiments is of noncollinear nature. The oxygen concentration is the responsible for the switching of the rotational sense of the spiral magnetic order found in oxygen-assisted Pt nanojunctions. Furthermore, the magnetic moments and magnetoresistances vary with oxygen concentration in the chain, which can be used to tune the magnetism and magnetotransport. The oxygen-assisted Pt nanojunctions offer a possibility for spintronic applications in magnetic memory and quantum devices.

Keywords: noncollinear magnetic order, magnetotransport, Pt nanojunction

(Some figures may appear in colour only in the online journal)

1. Introduction

The magnetic order and novel transport properties [1, 2] of transition metal nanojunctions have potential applications in future spintronic devices. These atomic scale junctions have been successfully fabricated utilizing the mechanically controllable break-junction technique [3, 4], which provide a platform to investigate quantum transport phenomena [5]. The experimental results show that late 5d elements, such as Pt and Au, can form a long chain [6]. More interesting, the probability of formation of atomic wires in break junctions can be significantly enhanced when some gas molecules, such as oxygen, are introduced in the growth of metal chain [7, 8]. The incorporation of oxygen atoms (rather than oxygen molecules) results in strong zigzag bonds with transition metal atom [9], assisting formation of a longer atomic wire. Thus the junction can survive for a long time [10] in a relatively low vacuum condition.

Bulk Pt is a non-magnetic metal, but Pt clusters [11], monoatomic chains [12] and nanojunctions [13] tend to spontaneously magnetize. The transition from non-magnetism to magnetism is triggered by the reduced coordination number (low dimensional) [14]. The magnetic properties of atomic contacts have been thoroughly explored [11–17] using density functional theory (DFT) calculations. It has been reported that local magnetic order of the stretched Pt atomic chains or contacts occurs with colossal magnetic anisotropy [11–17]. The theoretical calculations demonstrated that spin–orbit coupling (SOC) has a great influence on the magnetic moment and the conductance in Pt junctions [13]. Furthermore, experimental measurements [1, 10] have been performed to determine the magnetic features of Pt junctions. In

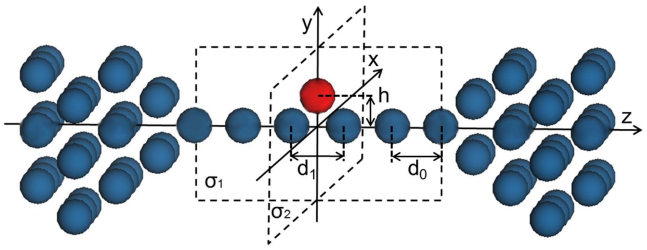

Figure 1. Structure of Pt atomic wire suspended between two Pt (001) pyramidal tips and O atom adsorbed at the bridge site. d_0 and d_1 give the Pt–Pt distance without and with oxygen, respectively. h denotes the height of O atom above the Pt–Pt bond. σ_1 and σ_2 are two mirror planes in oxygen-assisted Pt nanojunction.

these attempts, Cespedes *et al* [10] has prepared oxygen-assisted Pt junctions. A small negative magnetoresistance (MR) is observed in a high vacuum and the MR changes sign with the increasing of the gas concentration. They reproduced the reversed sign of the MR by utilizing DFT calculations without SOC, but the MR ratios are not consistent with the values detected in the experiments. Based on scalar relativistic calculations, the collinear magnetic alignment of Pt contact is presumed. However, the theoretical explanation is not correct. As is known, the spin alignment usually tends to be noncollinear in the system with SOC and inversion asymmetry [18], such as zigzag chains [19] consisting of 3d and 5d transition metal atoms. Importantly, a chiral magnetic order can be caused by Dzyaloshinskii–Moriya interaction (DMI) [20, 21] owing to SOC and inversion asymmetry. In order to fully understand the above experimental results, it is desirable to study magnetic order and electronic transport of oxygen-assisted Pt nanojunctions by explicitly considering SOC effects [22].

2. Geometries and computational details

The nanojunctions are modeled by a series of finite atomic wires suspended between two Pt electrodes, respectively. The electrode is selected with Pt (001) pyramidal tip. A 3×3 supercell (8.323×8.323 Å^2) is used in the direction perpendicular to the axial direction. The atoms in the lead slabs are fixed at their bulk position. The distances of Pt–Pt bond at pyramidal tip (about 2.64 Å) are smaller than the bulk value (2.77 Å). For the sake of clarity the Pt nanojunctions are represented by Pt_4O_N ($N = 0$, 1, 2, 3, 4 and 5), where N denotes the number of O atoms embedded in the nanojunctions. The clean Pt junction (Pt_4O_0) consists of a pure Pt atomic wire with four Pt atoms. The distance of Pt–Pt (d_0) bond of Pt atomic wire is set to be 2.43 Å. For the dirty Pt nanojunctions, all O atoms are adsorbed at the bridge sites of Pt wires. The dirty Pt junction with one O atom (Pt_4O_1) is shown in figure 1. The incorporation of the O atom increases the Pt–Pt distance to $d_1 = 2.60$ Å and the height of the O atom above the Pt wires (h) is 1.5 Å. These values of bond lengths are obtained using DFT calculations by Cespedes *et al* [10]. When $N = 2$, the suspended segment becomes a finite Pt_2O wire for the nanojunction Pt_4O_2. While the nanojunction with five O atoms (Pt_4O_5) develops into a contact with a finite PtO wire suspended between two Pt electrodes.

The electronic structure calculations are performed using the Vienna *ab initio* Simulation Package [23]. DFT calculations are performed with a cut-off energy of 400 eV. Exchange correlation potential with general gradient approximations in the form of Perdew–Burke–Ernzerhof [24] is chosen. The supercell along the axial direction is very large, hence the Brillouin zone in this direction is chose only at $k_z = 0$. While the Brillouin zone is sampled by a 4×4 k-point mesh in the plane perpendicular to the axial direction. In addition, the convergence criterion of total energy is set to be 10^{-6} eV. The initial magnetic moments in all junctions are set parallel to the Pt atomic wire. The magnetic structures are determined in a self-consistent manner which allows the magnitude and direction of magnetic moments to be fully relaxed. The ballistic conductance calculations are done using the PWCOND code of QUANTUM-ESPRESSO package [25]. The conductance is calculated by the Landauer–Buttiker formula,

$$G = \frac{e^2}{h} T(E_F), \tag{1}$$

where the total transmission at the Fermi level is obtained as $T(E_F) = \mathrm{Tr}[\mathbf{t}^{\dagger}\mathbf{t}]$.

3. Results and discussions

The clean Pt junction (Pt_4O_0) forms a local magnetic moment as shown in figure 2(a). The corresponding magnetic moments per layer are presented. The arrangement of magnetic moments is inserted in figure 2(a). It is clear that collinear magnetic structure aligning to nanowire is energetically stable and the magnitude distributes nonuniformly in the suspended segment. The spin magnetic moment of atom 4 and atom 5 is up to 0.48 μ_B, which is slightly larger than the value (0.41 μ_B) for the infinite wire with interatomic distance of 2.43 Å [10, 12, 14]. The tiny increase of spin moment may be due to low dimensionality. The magnetic moment of the atom 3 and atom 6 is 0.31 μ_B. However, the spin moment of apex atom is only 0.04 μ_B. The coordination number increases for the apex atom comparing to the central atoms, which generates a stronger coupling with the nonmagnetic electrode. As a result, the magnetic moment is significantly suppressed by the lead. The orbital magnetic moments are slightly smaller than spin moments and its distribution resembles to spin moments. These collinear results are similar with theoretical results of Smogunov *et al* [13]. The projected densities of states (PDOS) on different suspended atoms are plotted in figures 2(b) and (c), respectively. The PDOS projected on 5d atomic orbit for atom 4 follows the nature of Pt atom in an infinite Pt wire [17]. As shown in figure 2(b), these d states can be divided into three groups due to the symmetry: Δ_2 (d_{z^2}), Δ_3 (d_{xz}, d_{yz}) and Δ_4 (d_{xy}, $d_{x^2-y^2}$). The majority and minority density of states are asymmetrical for all atomic orbits, inducing a moderate moment. A small splitting of Δ_4 bands between the d_{xy} and $d_{x^2-y^2}$ states can be clearly seen in

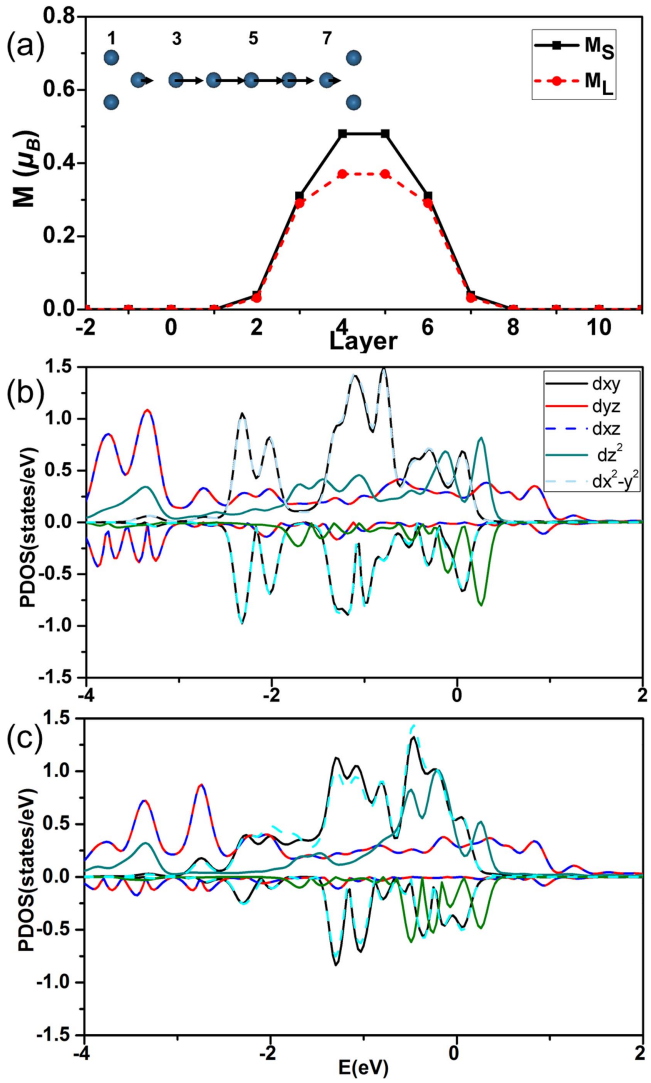

Figure 2. (a) The magnetic moments per atom of Pt_4O_0, black squares and red circles represent the spin and orbital moments, respectively. Inset: the alignments of magnetic moments in junction. Spin-decomposed projected densities of states (PDOS) for the suspended Pt atom 4 (b) and atom 3 (c).

the PDOS of atom 3 (figure 2(c)) thanks to the presence of the leads. The PDOS for both majority and minority states rearrange in these atomic orbits, leading to a slight decline of the magnetic moment in contrast to the central atom.

Previous theoretical results show that gas impurities can enhance the stability of atomic wires, and change the magnetic moment of break junctions [9, 26]. The magnetic properties of the dirty Pt nanojunctions are investigated here in order to shed light on the influence of oxygen impurities on Pt nanojunctions. The magnetic properties of the Pt junction incorporated with single O atom (Pt_4O_1) are depicted in figure 3(a). The profiles of spin and orbital magnetic moments are illustrated in the two insets, respectively. Interestingly, the local magnetic moments of Pt atoms are not parallel to the axis of nanowire any more. Noncollinear magnetic order displays in both spin and orbital magnetic moments. The alignment of magnetic moments is left-handed cycloidal spiral structures. The spin and orbital magnetic moments of the suspended Pt atoms decrease dramatically in contrast with the clean Pt junction. The spin magnetic moments of the atom 3 and atom 4 drop down to 0.15 μ_B and 0.18 μ_B, respectively. The values of orbital magnetic moments for Pt atom are similar with their spin moments. The spin magnetic moment of the O atom is 0.16 μ_B, while the value of orbital magnetic moment for the O atom is only 0.01 μ_B. From the electron difference density shown in figure 3(b), it is obvious that the electrons transfer from atom 4 and atom 6 to the O atom because of the high electronegativity of the O atom. The electron depletion of atom 4 and atom 6 gives rise to the decline of the magnetic moment in these atoms. The strong hybridization between the O and Pt atoms causes the magnetization of the O atom. In addition, some electrons transfer from atom 3 and atom 7 to the apex atom. It indicated that the coupling between the wire and the nonmagnetic electrode is enhanced, which results in a stronger suppression of magnetic moments for atom 3 and atom 7.

The magnetic profile of Pt_4O_2 is depicted in figure 3(c). The spin magnetic moments of the central Pt atoms and O atoms are 0.19 μ_B and 0.15 μ_B, respectively. The value for the central Pt atom is slightly larger than that of the infinite Pt_2O wire (0.15 μ_B). This effect is similar with the results of clean Pt nanojunction. But the value for the O atom is near to that for Pt_2O wire (0.16 μ_B). The moment for atom 3 and atom 8 drops down to 0.09 μ_B. The orbital magnetic moments for the suspended Pt atoms are about 0.08 μ_B and the values are near zero for two O atoms. Left-handed cycloidal spiral structure remains in this system and the deflection angle of magnetic moments is larger than Pt_4O_1. The angle for the apex atom is even up to 69°. When the number of the O atom increases to 5 (figure 3(d)), the spin magnetic moments of the Pt and O atoms in the center are 0.74 and 0.53 μ_B, corresponding to the value of the infinite PtO wire. The two remaining suspended Pt atoms have a spin moment of 0.38 μ_B. The spin moment even spreads to electrodes and the value of apex atom is up to 0.10 μ_B. The orbital magnetic moments for the suspended Pt atoms are almost half of the spin moments. But the values for all O atoms are close to zero. Noncollinear magnetic order also exists in this case, but the cycloidal spiral structure is not left-handed any more. Actually, the cycloidal spiral structure turns into right-handed when N increases to 4 and 5.

The influences of different oxygen concentration on the magnetic properties are explored. Total magnetic moments of the Pt junctions are depicted in figure 4(a) for both spin and orbital magnetic moments. One can find the total spin magnetic moments of the junctions show a unique nonmonotonous variation with N. The total spin moment decreases from $N = 0$ to $N = 2$ but immediately appears a reversal behavior, and it begins to increase when $N = 3$. When N is equal to 5, the total spin moment is up to 4.50 μ_B which is far greater than that in Pt_4O_2 (0.58 μ_B) and Pt_4O_0 (1.56 μ_B). Although the change for orbital moments is less evident than spin moments, the tendency is similar with that of spin moments. From the above description of the magnetic moment for Pt_4O_N, it is evident that the moments are mainly contributed by the suspended wires which reserve the nature of infinite wires. The magnetic moments for the central atoms

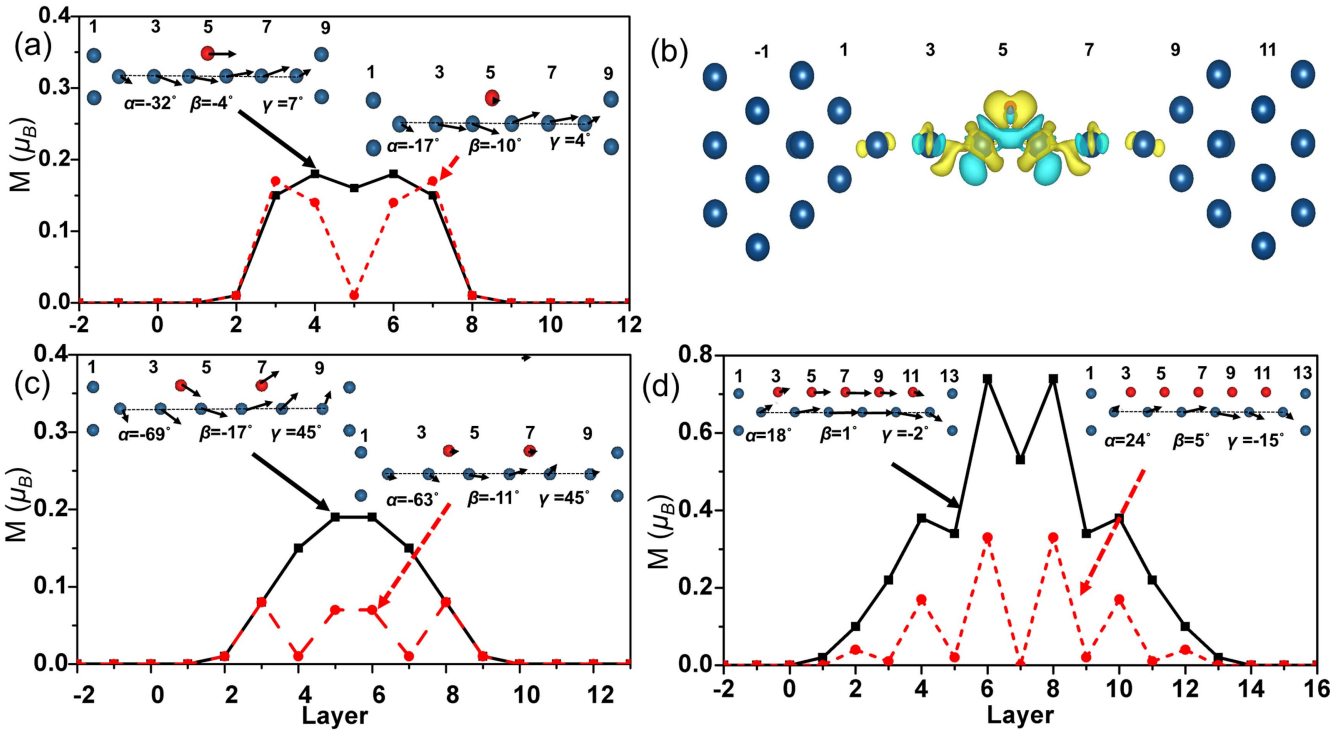

Figure 3. The corresponding magnetic moments per atom of (a) Pt_4O_1 (c) Pt_4O_2 and (d) Pt_4O_5. Inset: the different alignments of magnetic moments in junction with different O atom number are shown at the top of the corresponding figure. α, β and γ are the deflection angle of magnetic moments at different sites. (b) The charge transfer of Pt_4O_1 as the difference between the charge density of the combined system (Pt_4O_1) and the densities of the individual components (i.e., Pt junction and O atom).

are close to that of the corresponding nanowires. For the cases of infinite wire, the magnetic moments decrease from Pt to Pt_2O wire and increase from Pt_2O to PtO wire. The trend of magnetic moments for oxygen-assisted Pt nanojunctions resembles that of the corresponding infinite wires. Moreover, the charge transfer from the electrode to the suspended wire will also influence the trend of magnetic moment which will be discussed below.

In order to explain the above complex magnetic order, an effective Hamiltonian of the magnetic system is introduced, which can be expressed as

$$H_{\text{eff}} = -J_{ij}\mathbf{S}_i \cdot \mathbf{S}_j + \mathbf{D}_{ij} \cdot (\mathbf{S}_i \times \mathbf{S}_j). \quad (2)$$

The former term in the right side is the Heisenberg exchange interaction and J_{ij} is the exchange coefficient. The isotropic interaction favors parallel or antiparallel magnetic order determined by J_{ij}. The latter is the DMI and the DM vectors $\mathbf{D}_{ij}$ determine simultaneously the strength and sign of DMI. The antisymmetric interaction prefers an orthogonal arrangement. The DMI arises from spin–orbit scattering of electrons in the inversion asymmetric system. In our system, Pt has a strong SOC effect as a heavy 5d element. The DMI does not appear in the clean Pt junction with inversion symmetric. While the adsorption of O atoms at the bridge site of Pt wire breaks the structural inversion symmetry, which leads to the appearance of DMI. The DMI gives rise to the chiral magnetic order in the oxygen-assisted nanojunction. The oxygen-assisted system has two mirror planes illustrated in figure 1. One mirror plane (σ_1) includes Pt atomic wire and the O atom. The other one (σ_2) perpendicular to Pt atomic wire passes through the O atom. This pattern meets the second and third Moriya' rules [21]. As a consequence, the DM vector is perpendicular to the mirror plane σ_1 (along the x direction). $\mathbf{D}_{ij}$ without component along the wire direction leads to cycloidal arrangement rather than helical spiral structure. The DM vector is proportional to SOC coefficient λ, and depends on the relative position of the O atom [27, 28]. The vector product $\mathbf{S}_i \times \mathbf{S}_j$ is parallel to $-$x axis in the system of Pt_4O_1, hence the DM vectors must be antiparallel to $-$x axis for achieving a minimum energy in the magnetic system. In this case, the sign of $\mathbf{D}_{ij}$ is positive. The cycloidal spiral structure turns into right-handed when N increases to 4 and 5. The change of the rotational sense indicates that the sign of $\mathbf{D}_{ij}$ reverses with the oxygen concentration. As shown in figure 4(b), the DMI in the clean Pt junction is zero. DMI appears with the participation of oxygen and its sign is positive in a low oxygen concentration. But the sign changes from positive to negative when the number of O atoms increases to 4 and 5.

To further unveil the trend of magnetic moment and the sign reversal of DMI, the charge transfer of the dirty Pt nanojunctions with different oxygen concentration is analyzed. The charge transfer depends on the oxygen concentration, which will change the occupancy of electron states and the coupling between the lead and suspended wire. The electron difference densities of Pt_4O_2, Pt_4O_3, Pt_4O_4 and Pt_4O_5 are displayed in figure 4(c). The electron transfers from the suspended wire to the apex atom for $N \leqslant 3$, when O atoms are introduced.

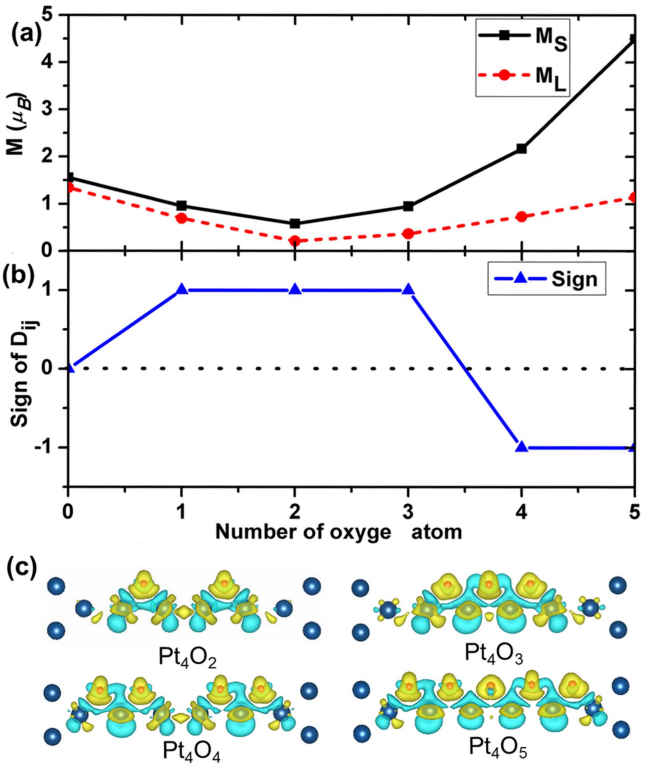

Figure 4. (a) Total magnetic moments of Pt junction as a function of O atom number, black solid squares and red solid circles stand for spin and orbital moments, respectively. (b) The sign of DM vector denoted by blue triangles depends strongly on O atom number. (c) The electron difference density of Pt_4O_2, Pt_4O_3, Pt_4O_4 and Pt_4O_5. electrodes, respectively. The portion of the lead slabs fixed at their bulk position do not show in this panel.

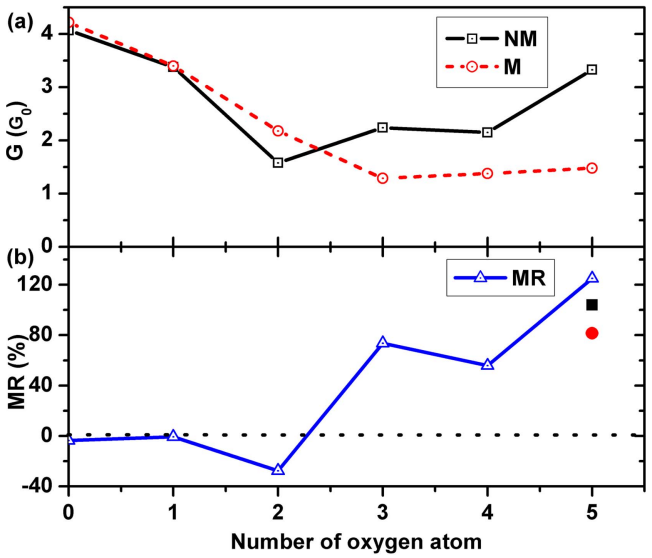

Figure 5. (a) The conductances of Pt junction change with O atom number, black open squares and red open circles represent nonmagnetic state and magnetic state, respectively. (b) Blue open triangles denote the MR of Pt_4O_N calculated with fully relativistic method. The values of Pt_4O_5 for scalar relativistic result and previous calculation result [10] are represented by red solid circle and black solid square, respectively.

The suppression of magnetic moments induced by the leads is strong. While $N = 4$ and $N = 5$, the apex atoms begin to lose electron. Hence some electron transfers back to the suspended segment at the situation of high oxygen concentration. The suppression of magnetic moments will become weaker. The magnetic moment will enhance in these systems. The sign of DMI clearly correlates with the charge transfer. One can find a significant change of the charge transfer for the apex atoms in Pt_4O_3 and Pt_4O_4 which leads to the sign reversal occurring between $N = 3$ and $N = 4$. The transition is similar with the helicity reversal of the skyrmion in alloys of helimagnets $Mn_{1-x}Fe_xGe$ [29, 30]. Recently, Belabbes *et al* [31] have also reported a similar effect. They have found that the magnitude and sign of the DMI can be modified by the coverage of the oxygen capping on the magnetic bilayer. They attributed the change of rotational sense to the variation of dipole moment, induced by the charge transfer and the hybridization between *d* state of the transition metal atom and *p* state of the O atom [31]. Oxygen concentration offers a convenient way to control the size and orientation of the magnetic moment in the Pt junction.

In experiments, different MR phenomena are detected in different gas concentration. A small negative MR is observed in a high vacuum and the sign of MR changes with increasing of gas concentration [10]. To get a better understanding of these complex MR phenomena, it is instructive to investigate the effect of noncollinear magnetic order on transport properties. Ballistic conductance by using fully relativistic calculation is presented in figure 5. The MR is estimated from the ratio $(G_{NM} - G_M)/G_M$, in which G_{NM} and G_M denote the conductance in nonmagnetic and magnetic state, respectively. For magnetic state, the conductance decreases with the number of oxygen atom and tends to be saturated until $N = 3$. Different from the magnetic state, the conductance for nonmagnetic case shows a growth trend when $N > 2$. The conductance of clean Pt junction for magnetic state (4.22 G_0) is the largest. Comparing with the magnetic case, a lower conductance for the nonmagnetic state (4.07 G_0) is obtained. Hence the MR in this case is negative (−3.7%). When a single O atom adsorbs on the Pt wire, the MR alters to −0.6%. These values are in agreement with the small negative MR observed in a high vacuum [10]. The conductance of Pt_4O_2 for magnetic state is 2.18 G_0, while the value for nonmagnetic case reaches its minimum (1.58 G_0). The negative MR is up to −27.5% in this system. When $N > 2$, the conductance for nonmagnetic state becomes larger than the magnetic case. Therefore, the MR of the nanocontact changes its sign and becomes positive. The growing gap of the conductance between nonmagnetic state (3.33 G_0) and magnetic state (1.48 G_0) gives rise to a large MR for $N = 5$. The MR is up to 125.0% for Pt_4O_5. This value is greater than our scalar relativistic value (81.0%) and the previous collinear calculation result [10]. It indicates that SOC plays an important role in magnetotransport of oxygen-assisted Pt nanojunctions.

In order to clarify the difference in the trend of the conductances between nonmagnetic and magnetic configurations and the change of the MR sign, a simple consideration

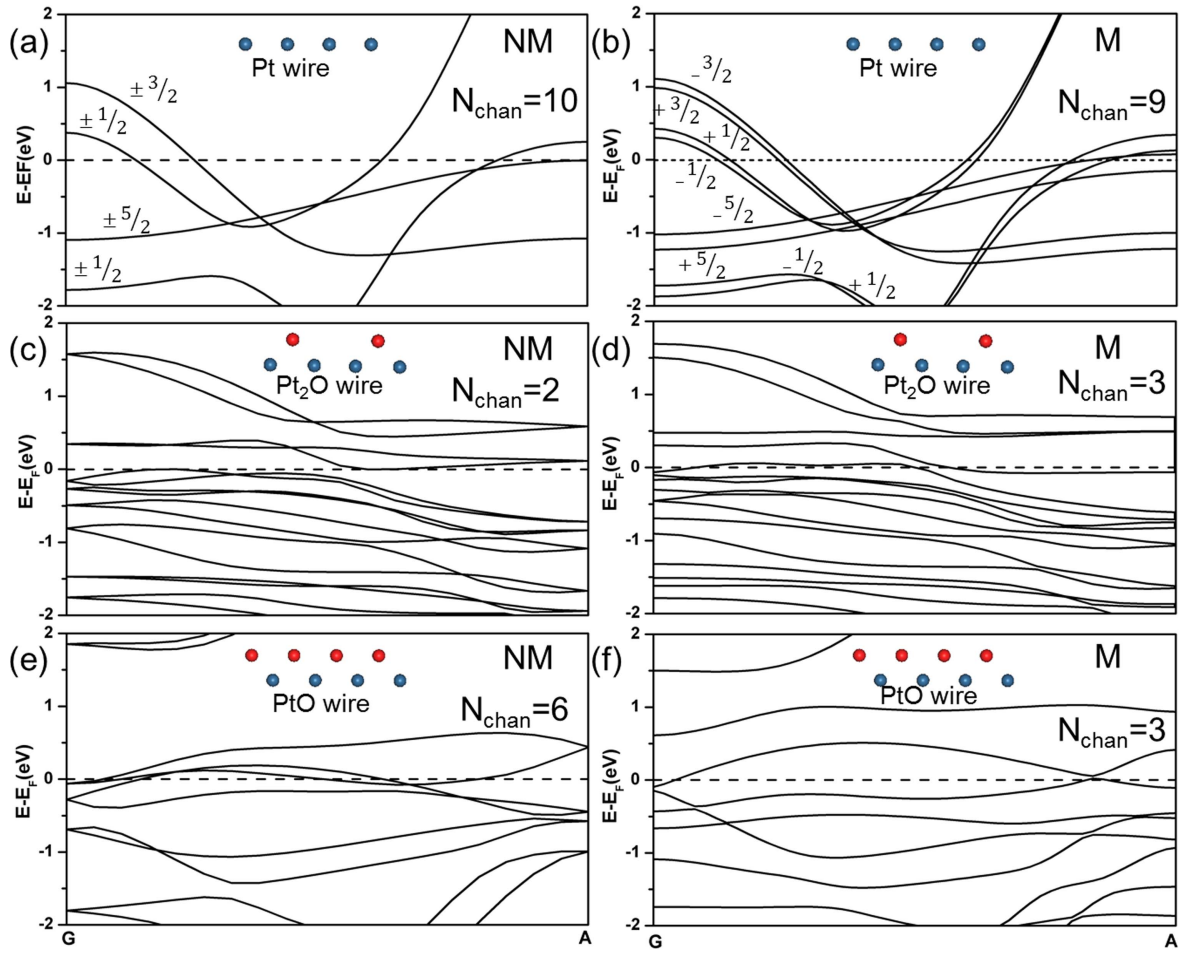

Figure 6. Band structures with both nonmagnetic and magnetic configurations of the ideal infinite Pt with $d = 2.43$ Å are shown in the upper panel (a) and (b). Pt_2O wire with both magnetic configurations are displayed (c) and (d). The two lower panels (e) and (f) show the bands for PtO wire. The schematic structure of the wires and the number of conductance channels are also provided in the corresponding panel.

of the band structures of the infinite Pt, Pt_2O and PtO wire is introduced. The bands for nonmagnetic state as well as for magnetic case are plotted in figure 6. The schematic structure of wires and the number of conductance channels (number of bands crossing the Fermi level) are also given in the corresponding figure. As shown in figures 6(a) and (b), the bands of Pt wires for both states are labeled by $m_j = \pm 1/2$, $\pm 3/2$ and $\pm 5/2$ (the eigenvalues of the operator $\mathbf{J}_z$). The bands for nonmagnetic state with $\pm m_j$ (figure 6(a)) are twofold degeneracy owing to time-reversal symmetry [13]. The degeneracy will disappear with the magnetization of the Pt wire (figure 6(b)). The number of conductance channels is ten for nonmagnetic state and nine for magnetic state, respectively. One can find that the bands $m_j = \pm 5/2$ for nonmagnetic state touch the Fermi level close to their very edges at A point, the electron occupying on these bands gives less contribution to conductance. Hence the similar conductances for both states occur even though the number of conductance channels for the nonmagnetic state is larger than that for the magnetic case. In low gas concentration, the adsorbed oxygen atom acts as a scatterer. A reduction of conductance is expected as soon as the scatterer (oxygen atom) is introduced. When $N = 2$, the segment suspended between two Pt electrodes is a finite Pt_2O wire. From the band structures of infinite Pt_2O (figures 6(c) and (d)), it is clear that the numbers of conductance channels are two for nonmagnetic state and three for magnetic state, which are far smaller than that of Pt wire. Accordingly, the negative MR occurs in Pt_4O_2 and the conductances of the nanojunctions for both states drop from $N = 0$ to $N = 2$. With increasing the gas concentration, the dirty Pt wire gradually behaves like finite PtO wire. Different from the infinite Pt_2O, the number of conductance channels for magnetic state ($N_{\text{chan}} = 3$) is smaller than the value for nonmagnetic case ($N_{\text{chan}} = 6$) in the system of the ideal infinite PtO wire. Consequently, a positive MR is expected in Pt_4O_5. The large gap of the number of conductance channels between nonmagnetic and magnetic states gives rise to the difference in the trends of the conductances between nonmagnetic and magnetic configurations for $N > 2$.

The conductances of Pt junctions are dependent on the oxygen concentration and magnetic state. The fully relativistic calculations reproduce the small negative MR detected in a high vacuum and explain the sign change of MR in experiments. Although the MR for fully relativistic calculation is larger than the previous scalar relativistic value for low vacuum, the large MR effects detected in experiments

[10] cannot be reproduced as before. The possible reason is that some sensitive factors are left out of consideration, like the temperature and kondo effect [32].

4. Conclusions

In summary, the magnetic order and electronic transport are explored in the oxygen-assisted Pt nanojunctions. The local magnetic order presents in clean nanocontacts along with a comparable orbital moment. DMI induces a noncollinear magnetic order in the oxygen-assisted nanocontacts. The spin rotational sense switches with the sign of DM vector which is determined by the oxygen concentration. The total magnetic moments vary as a function of oxygen concentration. In addition, the results of ballistic conductance calculations demonstrate that the conductance depends strongly on the magnetic state and the number of O atoms, thus MR can be tuned by oxygen concentration. The adsorption of O atoms provides new opportunities to manipulate the magnetic state and conductance in atomic scale. We expect these effects can be extended to other light *p* impurities such as C, N and F. The gas-assisted Pt nanojunctions are helpful for application in the magnetic memory and sensor devices.

Acknowledgments

This work is supported by the National Natural Science Foundation of China (NSFC11504178, NSFC11374162 and NSFC11247033), the Natural Science Foundation of Jiangsu Province (BK20150825), the Scientific Research Foundation of Nanjing University of Posts and Telecommunications (NY214010), and the Fundamental Research Funds for the Central Universities (NS2014073). J R Yuan would like to thank the Funding of Jiangsu Innovation Program for Graduate Education (KYZZ16_0166).

References

[1] Strigl F, Espy C, Bückle M, Scheer E and Pietsch T 2015 *Nat. Commun.* **6** 6172
[2] Kumar M, Tal O, Smit R H, Smogunov A, Tosatti E and van Ruitenbeek J M 2013 *Phys. Rev.* B **88** 245431
[3] Li C Z, Bogozi A, Huang W and Tao N J 1999 *Nanotechnology* **10** 221
[4] Vardimon R, Yelin T, Klionsky M, Sarkar S, Biller A, Kronik L and Tal O 2014 *Nano Lett.* **14** 2988
[5] Foti G and Vzquez H 2016 *Nanotechnology* **27** 125702
[6] Thiess A, Mokrousov Y, Blügel S and Heinze S 2008 *Nano Lett.* **8** 2144
[7] Thijssen W H A, Strange M, aan de Brugh J M J and van Ruitenbeek J M 2008 *New J. Phys.* **10** 033005
[8] Di Napoli S, Thiess A, Blügel S and Mokrousov Y 2014 *J. Phys.: Condens. Matter* **26** 295302
[9] Zhang C, Barnett R N and Landman U 2008 *Phys. Rev. Lett.* **100** 046801
[10] Cespedes O, Wheeler M, Moorsom T and Viret M 2014 *Nano Lett.* **15** 45
[11] Fernández-Seivane L and Ferrer J 2007 *Phys. Rev. Lett.* **99** 183401
[12] Smogunov A, Dal Corso A, Delin A, Weht R and Tosatti E 2008 *Nat. Nanotechnol.* **3** 22
[13] Smogunov A, Dal Corso A, Delin A, Delin A and Tosatti E 2008 *Phys. Rev.* B **78** 014423
[14] Delin A and Tosatti E 2004 *Surf. Sci.* **566** 262
[15] Negulyaev N N, Dorantes-Dvila J, Niebergall L, Jurez-Reyes L, Pastor G M and Stepanyuk V S 2013 *Phys. Rev.* B **87** 054425
[16] Bergman A *et al* 2016 arXiv:1604.00626
[17] Thiess A, Mokrousov Y and Heinze S 2010 *Phys. Rev.* B **81** 054433
[18] Bode M, Heide H, Von Bergmann K, Ferriani P, Heinze S, Bihlmayer G, Kubetzka A, Pietzsch O, Blügel S and Wiesendanger R 2007 *Nature* **447** 190
[19] Kashid V, Schena T, Zimmermann B, Mokrousov Y, Blügel S, Shah V and Salunke H G 2014 *Phys. Rev.* B **90** 054412
[20] Dzialoshinskii I E 1957 *Sov. Phys.—JETP* **5** 1259
[21] Moriya T 1960 *Phys. Rev.* **120** 91
[22] Otte F 2016 *Doctoral Dissertation* Christian-Albrechts Universität Kiel
[23] Kresse G and Furthmüller J 1996 *Comput. Mater. Sci.* **6** 15
[24] Perdew J P, Burke K and Ernzerhof M 1996 *Phys. Rev. Lett.* **77** 3865
[25] Giannozzi P *et al* 2009 *J. Phys.: Condens. Matter* **21** 395502
[26] Zheng X L, Xie Y Q, Ye X and Ke S H 2015 *J. Appl. Phys.* **117** 043902
[27] Cheong S W and Mostovoy M 2007 *Nat. Mater.* **6** 13
[28] Keffer F 1962 *Phys. Rev.* **126** 896
[29] Shibata K, Yu X Z, Hara T, Morikawa D, Kanazawa N, Kimoto K, Ishiwata S, Matsui Y and Tokura Y 2013 *Nat. Nanotechnol.* **8** 723
[30] Koretsune T, Nagaosa N and Arita R 2015 *Sci. Rep.* **5** 13302
[31] Belabbes A, Bihlmayer G, Blügel S and Manchon A 2016 *Sci. Rep.* **6** 24634
[32] Lucignano P, Mazzarello R, Smogunov A, Michele F and Erio T 2009 *Nat. Mater.* **8** 563